Bull. Mater. Sci., Vol. 40, No. 7, December 2017, pp. 1319–1328
https://doi.org/10.1007/s12034-017-1494-x

Synthesis of Ag_2Se–graphene–TiO_2 nanocomposite and analysis of photocatalytic activity of CO_2 reduction to CH_3OH

ASGHAR ALI and WON-CHUN OH*
Department of Advanced Materials Science and Engineering, Hanseo University, Seosan 31962, Korea
*Author for correspondence (wc_oh@hanseo.ac.kr)

MS received 23 November 2016; accepted 20 March 2017; published online 16 November 2017

Abstract. The present work deals with the development of a new ternary composite, Ag_2Se–G–TiO_2, using ultrasonic techniques as well as X-ray diffraction (XRD), scanning electron microscopy (SEM), high transmission electron microscopy (HTEM), X-ray photoelectron spectroscopy (XPS), Raman spectroscopy and UV–Vis diffuse reflectance spectra (DRS) analyses. The photocatalytic potential of nanocomposites is examined for CO_2 reduction to methanol under ultraviolet (UV) and visible light irradiation. Ag_2Se–TiO_2 with an optimum loading graphene of 10 wt% exhibited the maximum photoactivity, obtaining a total CH_3OH yield of 3.52 μmol g^{-1} h^{-1} after 48 h. This outstanding photoreduction activity is due to the positive synergistic relation between Ag_2Se and graphene components in our heterogeneous system.

Keywords. Graphene; photoreduction CO_2; semiconductors; CH_3OH; scavenger effect.

1. Introduction

In recent years, the significant increasing energy demand has been driven by growing world population. These days, the energy demand mostly depends on fossil fuels. Using fossil fuels produces greenhouse gases, which play the key role in global warming [1,2]. To overcome this problem, scientists are attempting to use alternative techniques to minimize the energy crisis and utilize CO_2. Three convenient approaches have been presented to reduce the amount of CO_2 in the atmosphere: (1) conversion of CO_2 into valuable solar fuels; (2) CO_2 capture and storage; and (3) CO_2 utilization [3–5]. Among these techniques, the photocatalytic reduction of CO_2 is the most promising technique to fulfil the energy crisis [6–10]. Although photocatalytic conversion of CO_2 using solar energy is the most convenient route for the transformation of CO_2, some barriers are involved in photocatalyitc CO_2 reduction: (1) fast recombination of photo-induced electron and hole recombination; (2) slow charge consumption during redox reaction; and (3) poor light utilization [1,11,12]. To overcome these barriers, scientists have developed new photocatalysts such as TiO_2, ZrO_2, ZnO, $ZnGa_2O_4$, $NaNbO_3$ and $SrTiO_3$, which have been vastly used for CO_2 photoreduction [13–17]. Among these photocatalysts, TiO_2 is a promising candidate for CO_2 photoreduction due to its unique properties, including low cost, chemical stability, nontoxicity and abundance [18]. However, its usage is limited due to its large band gap (3.2 eV) and fast charge carrier recombination [19,20]. Consequently, to enhance the efficiency of TiO_2 towards CO_2 photoreduction, various methods have been used such as doping of metals or their oxides (e.g., Cu [21], Ag [22] and Pd [23] when these metals fill the interstitial sites) and replacing Ti in the substitutional sites or agglomerates formation on the surface of TiO_2, thus, changing the properties of TiO_2 [24]. Moreover, graphene is very easy to obtain from low-cost graphite using the Hummers method [25,26]. Owing to its unique properties (surface functionalities, large surface area and stability), graphene is a suitable candidate to anchor on the surface of semiconductor materials (TiO_2) and promote the charge transfer mechanism. The oxygen functionalities modify the particle size and shape of the semiconductor materials on the surface of graphene. Chen *et al* [27] reported that graphene is an excellent supporter to anchor TiO_2 nanocrystals for the graphene–TiO_2 synthesis, because graphene acts as a photosensitizer to enhance the light response of TiO_2 towards the visible range of the electromagnetic spectrum. Further, due to its unique electronic and optical properties, metal selenide has attracted considerable attention over the past few decades. Metal selenide has been coupled with large band gap semiconductors (TiO_2), which enhanced the photocatalytic efficiency [28]. Silver selenide is available in two different phases (α-Ag_2Se, high temperature phase and β-Ag_2Se, low temperature phase) with the phase transition point at 1331°C [29]. α-Ag_2Se is a known superionic conductor and is mostly used as a solid electrolyte in photorechargeable secondary batteries, while β-Ag_2Se is broadly used in thermalchromic materials as a photosensitizer due to its narrow band gap [30,31]. Zheo *et al* [32] prepared a TiO_2/Ag_2Se nanocomposite by interface reaction and their result suggested that the nanocomposite is an excellent photovoltaic with photocurrent properties towards visible light. On the other hand, Cao *et al* [33] incorporated a single-crystalline Ag_2Se complex nanostructure using

solvothermal techniques, the result of which indicated that the nanostructure has an excellent photocatalytic activity by the photodegradation of rhodanmin B (RhB) dye using UV light irradiation. Here, we study a G–Ag_2Se–TiO_2 photocatalyst using an ultrasonication technique, and synthesize a nanocomposite characterized by X-ray diffraction (XRD), scanning electron microscopy (SEM), high transmission electron microscopy (HTEM), X-ray photoelectron spectroscopy (XPS), diffuse reflectance spectroscopy (DRS) and Raman spectroscopy. The main aim of this paper is to demonstrate an excellent photocatalytic-reduction ability of CO_2 with Ag_2Se–G–TiO_2 nanocomposites under light irradiation.

2. Experimental

2.1 *Materials*

Silver nitrate ($AgNO_3$), selenium powder (Se, 99%), ammonium hydroxide (NH_4OH, 25–28%), sodium sulfite ($Na_2SO_3 \cdot 7H_2O$, 95%), and titanium (IV) *n*-butoxide (TNB, $C_{16}H_{36}O_4Ti$) were purchased from Duksan Pure Chemicals Co. Ltd., Republic of Korea. All chemicals were used without further purification. All solutions were used with distilled water.

2.2 *Preparation of Ag_2Se–graphene–TiO_2 composite*

Typical preparations of G–Ag_2Se–TiO_2 nanocomposite are as follows. Three grams of Na_2SO_3 and 0.3 g of selenium power (Se) were mixed with 50 ml DI water and refluxed for 2 h to form Na_2SeSO_3 i.e., solution A. Then, 400 mg graphene oxide (GO) (which was prepared in the laboratory following the Hummers-Offeman method as reported in previous work) [34] and $AgNO_3$ (0.02 g) were mixed in 60 ml ethylene glycol by ultrasonication for 3 h to form a graphene oxide nanosheet (GONS)/Ag^{+2} i.e., solution B. Solutions A and B were then mixed and heated at 60°C for 30 min to obtain a homogenous solution. Finally, the molar ratios of ethanol:H_2O:TNB = 35:15:4 were added to the obtained solution and sonicated at room temperature for 2 h using a controllable serial-ultrasonic apparatus (Ultrasonic Processor, VCX 750, 500 Watt, Korea, Power 500 Watt, frequency 20 kHz, amplitude 50% and low intensity). The reaction solution was then left to cool and settle at room temperature after filtering with 47 mm Whatman filter paper at a pore size of 0.7 mm. The resultant powder was washed with distilled water five times, and dried in a vacuum oven at 100°C for 12 h; the solution was then transferred to an electric furnace for heat treatment at 500°C for 2 h. The same procedure was followed for the other control samples of Ag_2Se and Ag_2Se–graphene. The prepared nanocomposites were named as Ag_2Se, Ag_2Se–graphene and Ag_2Se–graphene–TiO_2.

2.3 *Photocatalytic reduction of CO_2*

In the photocatalytic experiments, the reduction of CO_2 with H_2O was carried out in a reactor designed in our laboratory reported in our pervious paper [35]. A typical reactor is comprised of a 500 W light irritation source (SOLAREDGE700, Perfect Light, China), closed chamber (with the dimensions of 20 cm length × 2.0 diameter), and carbon dioxide (CO_2) and nitrogen (N_2) gas (N_2 gas was used to remove gases from the reactor). One-hundred and fifty milligrams of the photocatalyst (Ag_2Se–G–TiO_2) and 0.05 moll^{-1} Na_2Se/Na_2S [36,37] were used as sacrificial reagents and added to 20 ml distillated water containing sodium bicarbonate ($NaHCO_3$, 0.04 M) and continually stirred for 2 h. Ultra-high-purity grade CO_2 gas was then purged through the reactor for 30 min. The suspension solution was then magnetically stirred and irradiated to visible light using a metal halide lamp (500 W, SOLAREDGE700, Perfect Light, China). The distance between the light source and photocatalyst was 10 cm. Moreover, the temperatures inside the reactor was maintained at 100°C using a heat sink. The reaction was continued for 2 d and at every 12 h interval, the reactor was left to cool naturally for CH_3OH desorption from the catalyst. Ten millilitres of the sample was then collected from the suspension solution using a syringe and a membrane filter. The collected sample was then analysed using gas chromatography (GC).

2.4 *Characterization*

The crystallinity and composition of the prepared samples were characterized using monochromatic high intensity CuK α radiation (λ = 1.5406 Å) in XRD (Shimadzu XD-D1). The surface state and structures of the prepared sample were examined using SEM (JS M-5600, JEOL, Japan) and TEM (JEM-2010, JEOL, Japan). XPS was performed using VG (Scientific VISACA Lab 2000), and a monochromatic Mg X-ray radiation source. Raman spectra of the prepared samples were observed using a spectrometer (Jasco Model Name NRS-3100) with an excitation laser wavelength of 532.06 nm.

3. Result and discussion

The phase structure of the prepared (Ag_2Se–G–TiO_2) nanocomposite was analysed by XRD. Figure 1 shows that the XRD pattern of Ag_2Se–G has diffraction peaks at around 2θ of 25.2, 30.88, 32.52, 34.63, 36.95, 39.98, 40.20, 42.65 and 43.38°, which can be indexed to the characteristic peak (101), (102), (120), (112), (121), (013), (122), (113) and (201) plane reflections, respectively, with orthorhombic Ag_2Se phase with a lattice parameter $a = 4.33$ Å, $b = c = 7.06$ Å (JCPDS PDF#00-024-1401) [38]. The TiO_2 peaks appeared at around $2\theta = 25.20$, 47.99, 53.82, 55.01, 62.62 and 68.75°, corresponding to the (101), (200), (105), (211), (204) and (116) diffractions as the anatase crystal phase with lattice parameter $a = b = 3.78$ Å and $c = 9.51$ Å (JCPDS PDF#00-021-1279). The TiO_2 (101) and graphene (002) peaks overlap each other in the same 2θ values; it is thus, very difficult to differentiate both peaks and the diffraction intensity peaks of the TiO_2 and graphene are very low, indicating that graphene oxides

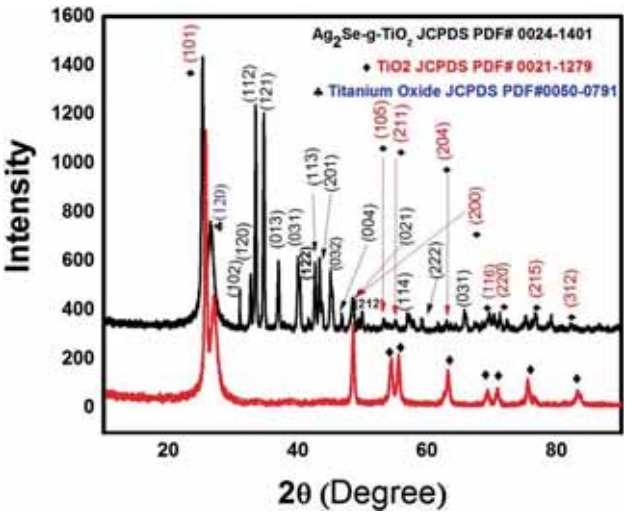

Figure 1. X-ray diffraction (XRD) patterns of Ag_2Se–G–TiO_2 composites.

are reduced to graphene [39,40]. Further, the fluctuation of diffraction peaks of the Ag_2Se–G–TiO_2 nanocomposites also demonstrates the increased amount of graphene and suppression of the crystalline phases. The compression in the peak intensity indicates that the lattice structure of Ag_2Se is distorted by the interaction with GO [41,42].

Figure 2a and b describes the overall morphology of the prepared sample obtained by SEM, which shows that the pure Ag_2Se particles are uniformly distributed on graphene oxide sheets, but the particle size and shape are difficult to distinguish in SEM. The graphene is shown as a sheet-like structure that is broken off in different directions, with a nanocomposite plate-like shape with a partial agglomerate; this plate-like structure demonstrated the existence of oxygen functionalities on the surface of the graphene [43]. Figure 2c and d shows the TiO_2 particles with an almost spherical shape, uniformly distributed on the graphene sheet. In addition, the final image clearly shows the difference between the binary and ternary composites. After the coupling of TiO_2, a bright spot appears in the ternary composite, showing that the synthesis of G–Ag_2Se–TiO_2 particles was successful and has a proper distribution pattern.

The microstructures of the Ag_2Se–G–TiO_2 were investigated by using high-resolution transmission electron microscopy (HRTEM). Figure 3 illustrates the HRTEM images of the prepared sample with different magnifications. The irregular dark images shown in figure 3a and b indicates that Ag_2Se was highly agglomerated, while TiO_2 nanoparticles were uniformly distributed on the graphene nanosheet, revealing the role of the Ag_2Se bridge-like support between TiO_2 and the graphene sheet [44,45]. Using the image J software, the average particle size of Ag_2Se ranges from

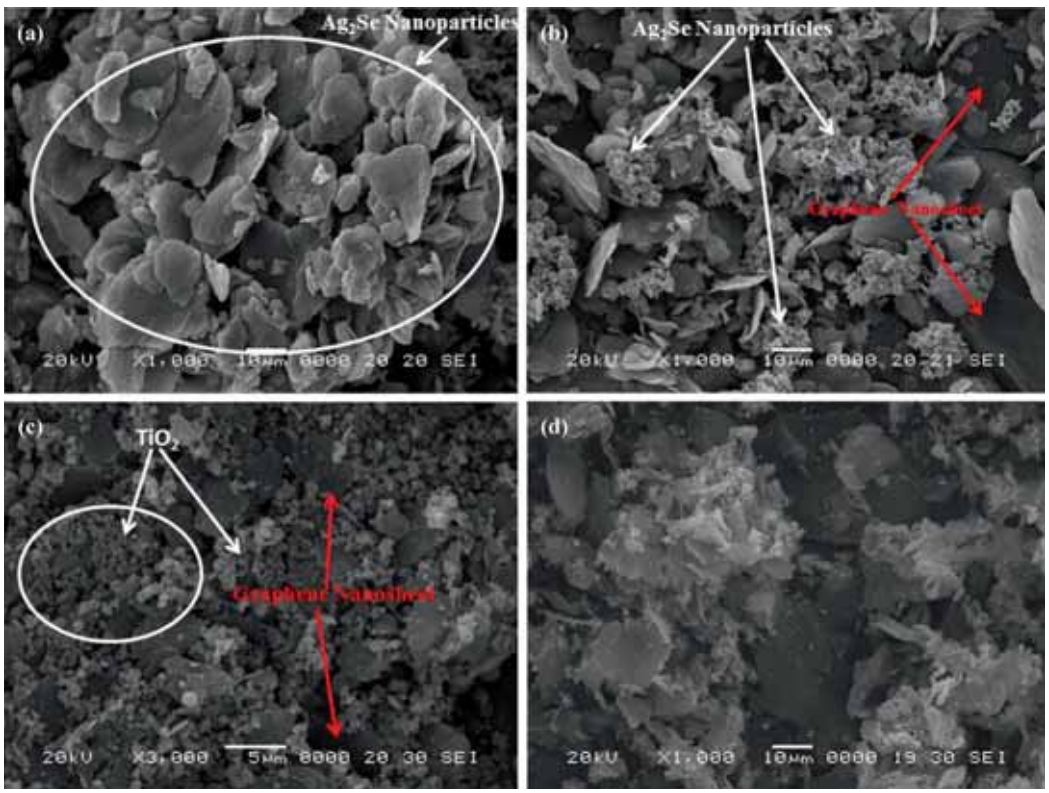

Figure 2. SEM image of Ag_2Se–G–TiO_2 composites (**a**) SEM images of Ag_2Se nanocomposites, (**b**) SEM images of Ag_2Se–G nanocomposites, (**c**) TiO_2 nanoparticles and (**d**) SEM images of Ag_2Se–G–TiO_2 nanocomposites.

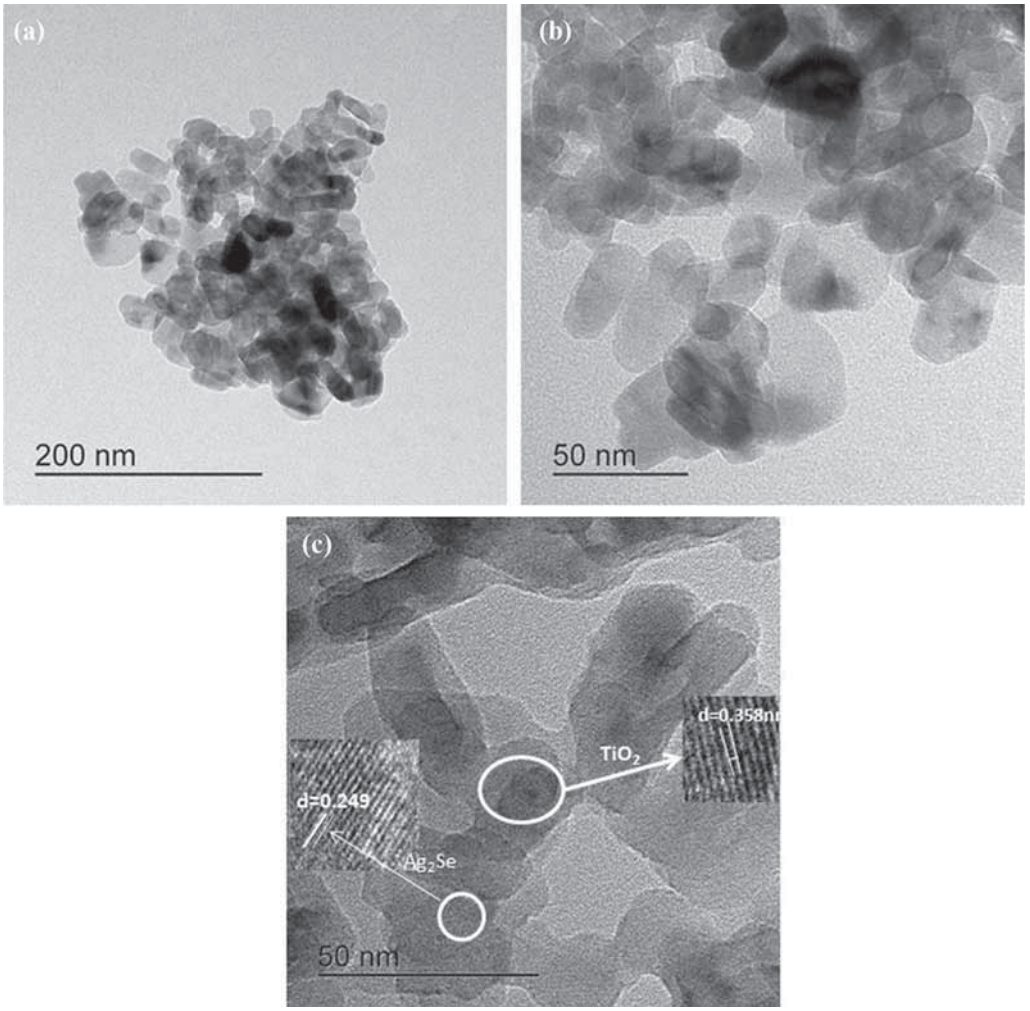

Figure 3. TEM image of Ag_2Se–G–TiO_2 composites with different magnification.

10–20 nm, and TiO_2 ranges from 12–40 nm. Figure 3c shows that the lattice spacing of the Ag_2Se is ∼0.249 nm, corresponding to the characteristic of the (013) crystal planes of β-Ag_2Se nanoparticles [33,46]. Also, the lattice spacing of the anatase TiO_2 phase is 0.35 nm [41,47]. Hence, the layered Ag_2Se supports the TiO_2 nanoparticles on the graphene sheet and provides a bridge between TiO_2 and the graphene nanosheet; we thus assume that an ultrasonication technique is favourable for enhancing the photocatalytic properties of the Ag_2Se–G–TiO_2 nanocomposite [48].

XPS was used to determine the chemical bonding and composition of the Ag_2Se–G–TiO_2 nanocomposite consisting of Ag_2Se, graphene and TiO_2. The XPS survey spectrum in figure 4a shows peaks corresponding to Ag, Se, O, C and Ti consistent with the formation of Ag_2Se–G–TiO_2 nanocomposites, while figure 4b and c shows the two main peaks of the Ag core level corresponding to $Ag2d_{3/2}$ and $Ag2d_{5/3}$ at 374 and 368 eV, respectively. The selenium Se3d binding energy peak located at 54.8 eV indicates the presence of oxidation state of Se^{+} [49,50]. From figure 4d, the C1s spectra show the presence of carbon in the Ag_2Se–G–TiO_2 composites. The C1s spectrum is located at 284.8 eV. The C1s binding energy shows C–O and C=O functional groups, which indicate that our prepared composites still contain partial oxygen functional groups [51]. These oxygen functional groups are beneficial for enhancing the light absorption towards the visible region [52]. The O1s peak is located at 531.75 eV from contributions of the C=O and O–C–OH groups (figure 4e). The O1s peak shows that after heat treatment, the conversion to other chemical species is also possible, and the other peak at 534 eV indicates that the C–OH group is still present [53–55]. Figure 4f shows the Ti2p peaks located at 459.8 and 465.7 eV, which indicate the Ti^{+4} oxidation state during synthesis, where the $Ti2p_{3/2}$ peak becomes narrow and its position changes, indicating the presence of some Ti in low valance (Ti^{+3}) form [55].

Further, Raman spectroscopy clearly illustrates the electronic structure of the carbon materials and the structural properties of Ag_2Se–G–TiO_2. Even a minor change in the band intensity and shifting provides the complete details

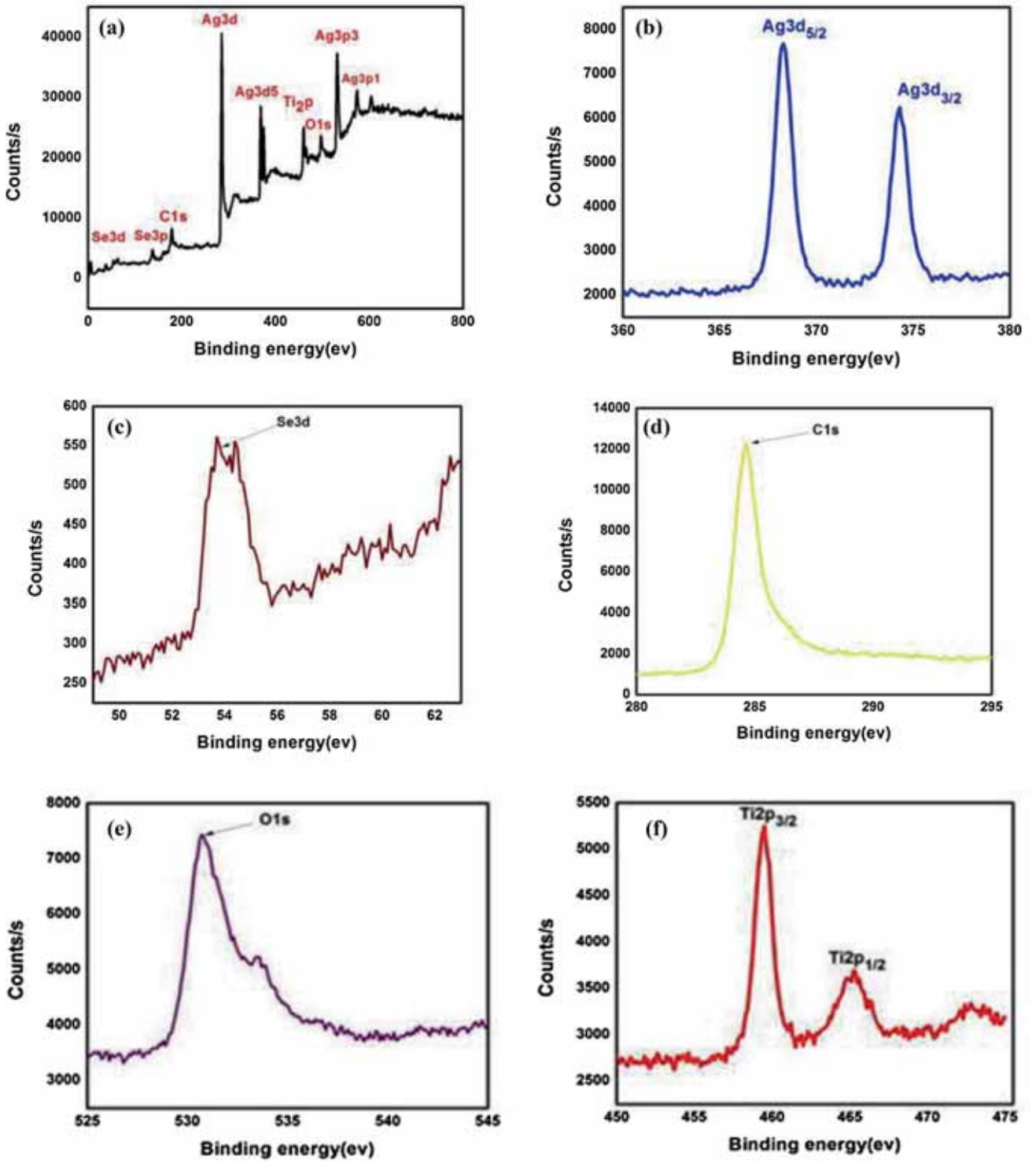

Figure 4. XPS results of the Ag_2Se–G–TiO_2 nanocomposite (**a**) survey scan spectra, (**b**) Ag peaks, (**c**) Se 3d, (**d**) C1s, (**e**) O1s and (**f**) Ti2p.

of the nature of carbon–carbon bonds and defects [41]. Figure 5 shows details on the graphene oxide and Ag_2Se–G–TiO_2 nanocomposites. The strong peak observed around at the 230 cm^{-1} wave could be due to the characteristic vibrations of the Ag_2Se band [56–58], while the peaks around 412 cm^{-1} show the presence of the anatase TiO_2 band [59]. The characteristic D band appears at 1354 cm^{-1}, revealing the disorder in the atomic arrangements. This indicates the increasing modes

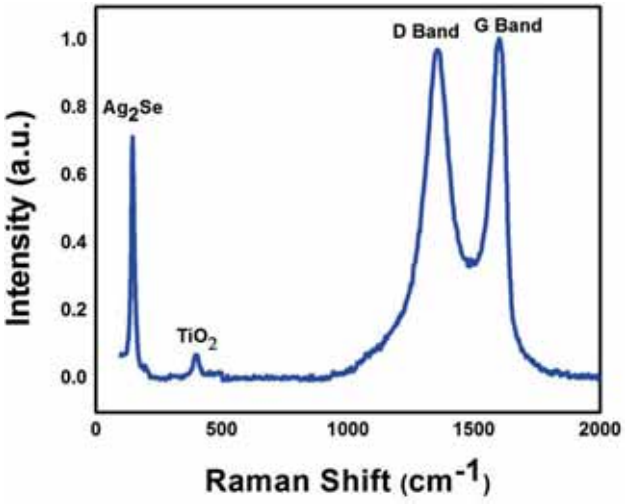

Figure 5. Raman spectra of Ag_2Se–G–TiO_2.

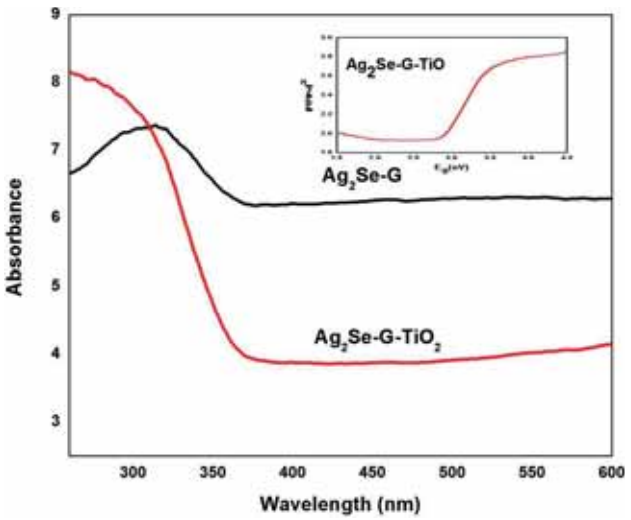

Figure 6. Diffuse reflectance spectra (DRS) obtained from Kubelka-Munk transformation function *vs.* photon energy of Ag_2Se–G and Ag_2Se–G–TiO_2.

of the sp^3 atoms in the carbon and the G bands appearing at 1584 cm^{-1}; this provides information on the in plane vibration of the sp^2 bonded carbons [60]. The nature of the defects can be determined from the intensity ratio of the corresponding D–G bands. The calculated ratios of the I_D and I_G bands are ~0.07. The intensity ratios of the D and G bands (I_D/I_G ratio) demonstrate that the graphene consists of several layers, as explained in the previously mentioned paper [61].

For the eradication of environmental pollutants, we need an ideal photocatalyst with a maximum efficiency (UV and visible) in the range of the electromagnetic spectrum. DRS is used to understand the absorption response in the Ag_2Se–G-TiO_2 nanocomposites to the electromagnetic spectrum. Figure 6 illustrates that our nanocomposites are mostly in the visible part of the electromagnetic spectrum and the total spectra are similar to carbon-based semiconductor materials [62]. Figure 6 shows that after the introduction of graphene with Ag_2Se and TiO_2, the absorption edge shifts towards the visible region. Due to the carbon-based structure of graphene, the unpaired π electron merges with the metal nanoparticles, causing a shift in the band edges and enhancing the light absorption towards the visible region. Therefore, the attachment of graphene with Ag_2Se and TiO_2 increases the absorption intensities in the entire visible region, confirming the improved efficiency of the light-harvesting activity as shown in figure 6. To calculate the band gap of the Ag_2Se–G–TiO_2 nanocomposite, the Kulbelka–Munk function $F(R) = (1 - R)^2/2R$ [63] is used. The obtained plot in figure 6 shows that the banding energy of the Ag_2Se–G–TiO_2 nanocomposites was 2.6 eV, which was almost less than that of pure TiO_2 and Ag_2Se. The reducing banding energy of the Ag_2Se–G–TiO_2 nanocomposite is due to the distribution of the Ag_2Se and TiO_2 nanocomposites on the graphene sheets. Moreover, the partial agglomeration can change the absorption property, reducing the band gap of the nanocomposite [64,65].

The yield of methanol according to the time of irradiation in the photocatalytic experiments is shown in figure 7a. The reaction quantum yield (QE) is estimated using the CH_3OH yield, considering that six electrons are required to reduce CO_2 to CH_3OH. The equation is as follows [66,67]:

$$2CO_2 + 4H_2O \rightarrow 2CH_3OH + 3O_2,$$

$$\Phi_{\text{Methanol}}\,(\%) = 100 \times (6 \times \text{ mole of } CH_3OH \text{ yield})/(\text{mole of photon absorbed by catalyte}) - \text{mole of photon} = (I \times S)/(N_A \times E),$$

where I is light intensity (0.12 mW cm^{-2}), S the irradiated area of the reactor (30 cm × 15 cm), E the photon energy (4.97×10^{-19} J at 400 nm) and N_A the avogadro number (6.02×10^{23} mol^{-1}).

The result reveals that the photocatalytic efficiency of TiO_2 can be greatly enhanced through the attachment of graphene and Ag_2Se to the TiO_2 structure. In addition, CH_3OH was detected as a major product from the photoreduction of CO_2 over the Ag_2Se–G–TiO_2 photocatalysts. The total methanol yield and quantum yield of the photocatalysts for 48 h using a UV/visible light source was calculated and are shown in table 1a and b. The photocatalytic reduction of CO_2 under UV light is more active than under visible light irradiation, and the maximum CH_3OH yield of Ag_2Se–G–TiO_2 after 48 h was found to be 1.3420 μmol $g^{-1}h^{-1}$ without using any sacrificial reagents. Further, to improve the catalytic activity of the photoreduction of CO_2, Na_2SO_3 is used as a scavenger as shown in figure 7b. Generally, Na_2SO_3 was used to increase the photocatalytic activity of the semiconductors and to avoid the oxidation of the reduction products in liquid phase. Na_2SO_3 is a highly efficient electron donor, which is used as a cycling electron donor to combine CO_2 photoreduction with water splitting to improve the overall efficiency [68].

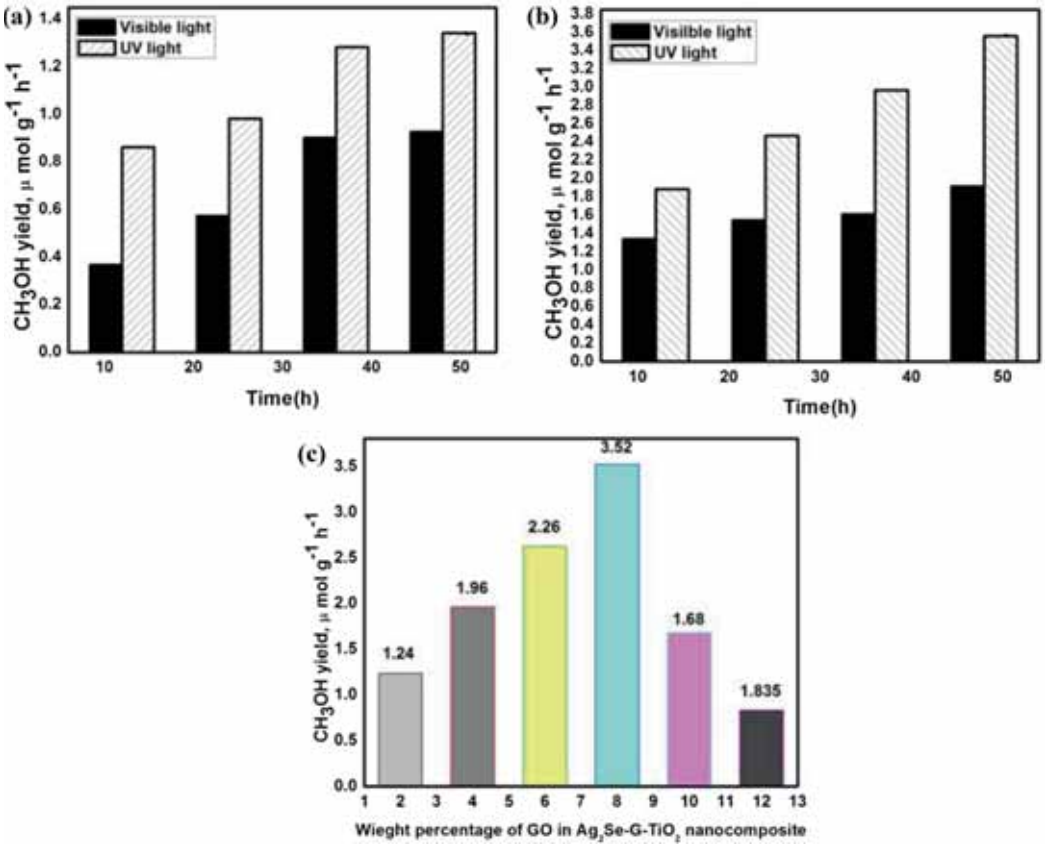

Figure 7. The methanol yield in the photocatalytic reduction of CO_2 under UV/visible light irradiation of different nanocomposites. (**a**) methanol yield under UV/visible light irradiation without scavenger, (**b**) methanol yield under UV/visible light irradiation using Na_2SO_3 and (**c**) weight percentage of graphene in Ag_2Se–G–TiO_2 nanocomposite.

Table 1. Effect of preparation method on methanol yield and quantum yield.

Sample	CH_3OH yield (μmol g^{-1} h^{-1})	Quantum yield (QE)
(a) *Visible light*		
Ag_2Se–G–TiO_2 (12 h)	0.3665	0.0530
Ag_2Se–G–TiO_2 (24 h)	0.5734	0.0770
Ag_2Se–G–TiO_2 (36 h)	0.9020	0.1487
Ag_2Se–G–TiO_2 (48 h)	0.9255	0.1504
(b) *UV light*		
Ag_2Se–G–TiO_2 (12 h)	0.8623	0.1395
Ag_2Se–G–TiO_2 (24 h)	0.9814	0.1647
Ag_2Se–G–TiO_2 (36 h)	1.2821	0.2090
Ag_2Se–G–TiO_2 (48 h)	1.3420	0.1522

Table 2. Effect of preparation method on methanol yield and quantum yield.

Sample after Na_2SO_3	CH_3OH yield (μmol $g^{-1}h^{-1}$)	Quantum yield (QE)
(a) *Visible light*		
Ag_2Se–G–TiO_2 (12 h)	1.3380	0.2237
Ag_2Se–G–TiO_2 (24 h)	1.5450	0.2054
Ag_2Se–G–TiO_2 (36 h)	1.6100	0.2613
Ag_2Se–G–TiO_2 (48 h)	1.9170	0.3141
(b) *UV light*		
Ag_2Se–G–TiO_2 (12 h)	1.8862	0.3061
Ag_2Se–G–TiO_2 (24 h)	2.4682	0.4005
Ag_2Se–G–TiO_2 (36 h)	2.9683	0.4817
Ag_2Se–G–TiO_2 (48 h)	3.5262	0.5722

The methanol yield of Ag_2Se–G–TiO_2 under UV (VL-4.LC, 8 W, 365 nm)/visible light is almost higher than that of without using a scavenger. The CH_3OH yield of Ag_2Se–G–TiO_2 with different time intervals is shown in table 2a and b. The photoreduction rate of the pure TiO_2 and Ag_2Se–graphene nanosheets is smaller than that of the Ag_2Se–G–TiO_2 nanocomposites. This shows that a strong interaction between graphene and the attached semiconductor materials, Ag_2Se supported by TiO_2, allows good interfacial contact with the graphene sheet by enhancing the synergistic effect between Ag_2Se and the

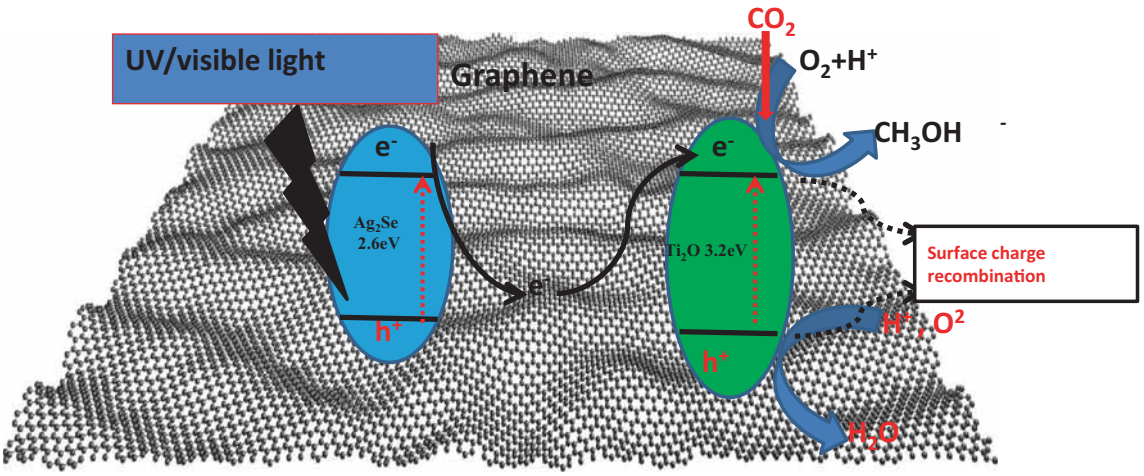

Figure 8. Mechanism study of photocatalytic reduction of CO_2.

graphene sheet, which plays an important role in photoreduction activity. Hence, graphene plays an important role in the catalytic photoreduction of CO_2. The optimum content of graphene in the Ag_2Se–G–TiO_2 system was found to be 8 wt% as shown in figure 7c. The further increase in the amount of graphene in the ternary system was found to decrease the photocatalytic performance, possibly due to the increased light absorption of graphene itself, which affects the excitation of Ag_2Se and TiO_2 in the composites [66].

Primarily, it is known that the photocatalyitc properties of semiconductors are due to the formation of photogenerated charge carrier (holes and electrons), which is due to the absorption of photon with energy greater or equal than the band energy (E_g) of separating the valence band (VB) from the conduction band (CB) [69,70]. From the proposed mechanism shown in figure 8 that the energy of the photon is equal or greater than the band gap energy (E_g), and thus, photogenerated electrons and holes diffuse to the surface of the semiconductor for desire chemical reaction; however, due to the absence of co-catalysts or lack of active sites, the number of excited electrons rapidly decreases. This increases the electron–hole recombination on the surface of the semiconductors. To overcome this deficiency and enhance the overall efficiency of the semiconductor, a different strategy needs to be used, such as doping of the nanostructure of the semiconductor, semiconductor heterojunction or nanocarbon material (graphene) on the semiconductor. This not only minimizes the recombination rate, but also enhances the visible light response. Further, metal ion (Ag) doping generates impurity levels in the forbidden region of the wide gap of TiO_2. In addition, the metal ion (Ag) can act as an electron trap and an active site for highly favourable CO_2 photoreduction; TiO_2 doped with silver has an excellent ability to reduce CO_2 to CH_3OH [71,72]. For better photocatalytic activity, a heterogeneous system needs to be introduced. The main advantage of the heterogeneous system is that it greatly improves the electron–hole separation and increases the lifetime of the charge carrier. Attachment of nanoparticles on the graphene sheet is helpful for converting CO_2 to CH_3OH [73] under the UV/visible light irradiation. The photogenerated electron in the VB of Ag_2Se easily transfers to the graphene sheet, which slows down the recombination of electron–hole pairs and enhances the electron transport to the catalytic sites for the reduction of CO_2. Due to its large surface area and various defective sites, graphene can easily absorb CO_2, and the photogenerated electron on Ag_2Se is then transferred to the active sites of graphene. The absorbed CO_2 is then reduced to CH_3OH [74]. The photocatalytic CO_2 reduction to convert the CH_3OH mechanism is expressed in equations (1–8).

$$TiO_2 + h\nu \rightarrow TiO_2\,(e^- + h^+), \tag{1}$$

$$TiO_2(h^+) + H_2O \rightarrow TiO_2 + H^+ + OH^\bullet, \tag{2}$$

$$TiO_2(e^-) + Ag_2Se \rightarrow TiO_2 + Ag_2Se\,(e^-), \tag{3}$$

$$Ag_2Se\,(e^-) + H^\bullet \rightarrow Ag_2Se + H^\bullet, \tag{4}$$

$$CO_2^+ + 2H^\bullet + 2e^- \rightarrow HCO_2H \text{ (formic acid)}, \tag{5}$$

$$CO_2 + 2H^\bullet + 2e^- \rightarrow CO + H_2O, \tag{6}$$

$$CO_2 + 4H^\bullet + 4e^- \rightarrow HCHO + H_2O \text{ (formaldehyde)}, \tag{7}$$

$$CO_2 + 6H^\bullet + 6e^- \rightarrow CH_3OH + H_2O \text{ (methanol)}. \tag{8}$$

Equations (1)–(4) explain the reaction mechanism of Ag_2Se, TiO_2 and graphene, exhibiting the production of the photoexcited electron–hole pair and their subsequent reaction (equations (5–8)) [75] reveal the oxidation and reduction processes, in which the holes are used for oxidation, while the electrons are used for the reduction of CO_2. In the photoreduction mechanism, the generated electron reacts with the dissolved oxygen modules and produces oxygen peroxides

radicals. The positive holes are absorbed in water, resulting in the production of hydroxyl radicals (OH) and hydrogen ions (H^+) and then reacts with the excited electrons, leading to the formation of $^{\bullet}H$, while CO_2 simultaneously reacts with the excited electron and CO_2^- is formed. $CO_2^{-\bullet}$ is finally converted to CH_3OH.

4. Conclusion

Heterogeneous Ag_2Se–G–TiO_2 was prepared using ultrasonic techniques. The SEM and HRTEM images of the prepared sample demonstrate that the Cu_2Se and TiO_2 are uniformly dispersed on graphene sheets. The average particle sizes of Ag_2Se ranged from 10 to 20 nm, while those of TiO_2 ranged from 12 to 40 nm. The attachment of Ag_2Se and graphene to TiO_2 improved the photocatalytic property of TiO_2, releasing and reducing CO_2 to CH_3OH. DRS results reveal that after the attachment of graphene to Ag_2Se and TiO_2, the absorption edge shifts towards the visible region, promoting an excited electron charge carrier, and the interface of Ag_2Se and graphene was found to be due to the synergistic effect of graphene and Ag_2Se by increasing the recombination time. It is also concluded that the different wt% also affected the photocatalytic efficiency. The optimum content was found to be 8 wt% and the maximum CH_3OH yield reached 3.523 $\mu mol\, g^{-1}\, h^{-1}$. It is expected that the present research will facilitate new methods of using graphene-based materials to promote an efficient heterosystem for CH_3OH production.

References

[1] Roy S C, Varghese O K, Paulose M and Grimes C A 2010 *ACS Nano*. **4** 1259
[2] Khatib H 2012 *Energ. Policy* **48** 737
[3] Windle C D and Perutz R N 2012 *Coordin. Chem. Rev.* **256** 2562
[4] Qu Y and Duan X 2012 *J. Mater. Chem.* **22** 16171
[5] Hurst T F, Cockerill T T and Florin N H 2012 *Energ. Environ. Sci.* **5** 7132
[6] Yu J, Low J, Xiao W, Zhou and Jaroniec M 2014 *J. Am. Chem. Soc.* **136** 8839
[7] Chen Y, Wang C, Sun P, Yang P, Du L and Mai W 2017 *Mater. Chem. A: Fuel* **37** 40
[8] Xiang Q, Cheng B and Yu J 2015 *Angewandte Chemie Int. Ed.* **54** 11350
[9] Kondratenko E V, Mul G, Baltrusaitis J, Larrazábal G O and Pérez-Ramírez 2013 *J. Energ. Environ. Sci.* **6** 3112
[10] Yuan L and Xu Y-J 2015 *Appl. Surf. Sci.* **342** 154
[11] Morris A J, Meyer G J and Fujita E 2009 *Acc. Chem. Res.* **42** 1983
[12] Habisreutinger S N, Schmidt-Mende L and Stolarczyk J K 2013 *Angewandte Chemie Int. Ed.* **52** 7372
[13] Tong H, Ouyang S, Bi Y, Umezawa N, Oshikiri M and Ye J 2012 *Adv. Mater.* **24** 229
[14] Mikkelsen M, Jørgensen M and Krebs F C 2010 *Energ. Environ. Sci.* **3** 43
[15] Zhang N, Ouyang S, Li P, Zhang Y, Xi G, Kako T and Ye J 2011 *Chem. Commun.* **47** 2041
[16] Yan S C, Ouyang S X, Gao J, Yang M, Feng J Y, Fan X X *et al* 2010 *Angewandte Chemie* **122** 6544
[17] Xu Y and Schoonen M A 2000 *Am. Mineral.* **85** 543
[18] Tan L L, Chai S P and Mohamed A R 2012 *Chem. Sus. Chem.* **5** 1868
[19] Nozik A 1975 *Nature* **257** 383
[20] Fujishima A and Honda K 1972 *Nature* **238** 37
[21] Nasution H W, Purnama E, Kosela S and Gunlazuardi 2005 *J. Catal. Commun.* **6** 313
[22] Murakami N, Saruwatari D, Tsubota T and Ohno T 2013 *Curr. Org. Chem.* **17** 2449
[23] Ishitani O, Inoue C, Suzuki Y and Ibusuki T 1993 *J. Photochem. Photobiol. A: Chem.* **72** 269
[24] Sahu M and Biswas P 2011 *Nanoscale Res. Lett.* **6** 1
[25] Hummers Jr W S and Offeman R E 1958 *J. Am. Chem. Soc.* **80** 1339
[26] Marcano D, Kosynkin D, Berlin J, Sinitskii A, Sun Z, Slesarev A *et al* 2010 *ACS Nano*. **4** 4806
[27] Chen C, Cai W, Long M, Zhou B, Wu Y, Wu D *et al* 2010 *ACS Nano*. **4** 6425
[28] Naether C, Scherb S and Bensch W 2003 *Acta Crystallogr. Sec. E: Struc. Rep. Online* **59** 280
[29] Das V D and Karunakaran D 1989 *Phys. Rev. B* **39** 10872
[30] Kobayashi M 1990 *Solid State Ionics* **39** 121
[31] Cui Y, Chen G, Ren J, Shao M, Xie Y and Qian Y 2003 *J. Solid State Chem*. **172** 17
[32] Zhao J, Jiang B, Zhang S, Niu H, Jin B and Tian Y 2009 *Sci. China Ser. B: Chem.* **52** 2213
[33] Cao H, Xiao Y, Lu Y, Yin J, Li B, Wu S and Wu X 2010 *Nano Res.* **3** 863
[34] Ullah K, Ali A, Ye S, Zhu L and Oh W-C 2015 *Sci. Adv. Mater.* **7** 606
[35] Ali A and Oh W-C 2016 *Nanotub. Carbon Nanostruc.* **24** 555
[36] Wang P-Q, Bai Y, Luo P-Y and Liu J-Y 2013 *Catal. Commun.* **38** 82
[37] Zhai Q, Xie S, Fan W, Zhang Q, Wang Y, Deng W and Wang Y 2013 *Angewandte Chemie* **125** 5888
[38] Zhan J, Yang J X, Li S, Wang D, Xie Y and Qian Y 2001 *Int. J. Inorg. Mater.* **3** 47
[39] Zhang X-Y, Li H P, Cui X L and Lin Y 2010 *J. Mater. Chem.* **20** 2801
[40] Zhang H, Lv X, Li Y, Wang Y and Li J 2009 *ACS Nano.* **4** 380
[41] Perera S D, Mariano R G, Vu K, Nour N, Seitz O, Chabal Y *et al* 2012 *ACS Catal*. **2** 949
[42] Pejova B 2014 *J. Solid State Chem.* **213** 22
[43] Glazov V, Pashinkin A and Fedorov V 2000 *Inorg. Mater.* **36** 641
[44] Toroker M C, Kanan D K, Alidoust N, Isseroff L Y, Liao P and Carter E A 2011 *Phys. Chem. Chem. Phys.* **13** 16644
[45] Zhuang H L and Hennig R G 2013 *J. Phys. Chem. C* **117** 20440
[46] Zhao L L, Gao Z-M, Liu H, Yang J, Qiao S-Z and Du X-W 2013 *CrystEngComm.* **15** 1685
[47] Ghosh T, Lee J-H, Meng Z-D, Ullah K, Park C-Y, Nikam V and Oh W C 2013 *Mater. Res. Bull.* **48** 1268
[48] Xiang Q, Yu J and Jaroniec M 2012 *J. Am. Chem. Soc*. **134** 6575

[49] Mishra S, Du D, Jeanneau E, Dappozze F, Guillard C, Zhang J *et al* 2016 *Chem.–Asian J*. **11** 1658
[50] Ge J P, Xu S, Liu L P and Li Y D 2006 *Chemistry—Eur. J.* **12** 3672
[51] Deka S, Genovese A, Zhang Y, Miszta K, Bertoni G, Krahne R *et al* 2010 *J. Am. Chem. Soc*. **132** 8912
[52] Dreyer D R, Park S, Bielawski C W and Ruoff R S 2010 *Chem. Soc. Rev.* **39** 228
[53] Zhang L F and Zhang C Y 2014 *Nanoscale* **6** 1782
[54] Szabó T, Berkesi O, Forgó P, Josepovits K, Sanakis Y, Petridis D *et al* 2006 *Chem. Mater*. **18** 2740
[55] Jeong H-K, Noh H-J, Kim J-Y, Jin M, Park C and Lee Y 2008 *EPL (Europhys. Lett.)* **82** 67004
[56] Naumov P, Barkalov O, Mirhosseini H, Felser C and Medvedev S 2016 *J. Phys.: Condens. Matter* **28** 385801
[57] Hamlin J, Jeffries J R, Butch N, Syers P, Zocco D, Weir S *et al* 2011 *J. Phys.: Condens. Matter* **24** 035602
[58] Azhniuk Y M, Dzhagan V, Raevskaya A, Stroyuk A, Kuchmiy S Y, Valakh M Y *et al* 2008 *J. Phys. Condens. Matter* **20** 455203
[59] Lange H, Artemyev M, Woggon U and Thomsen C 2008 *Nanotechnology* **20** 045705
[60] Ferrari A C 2007 *Solid State Commun.* **143** 47
[61] Chen W C, Wen T C and Gopalan A 2002 *Synth. Metals* **128** 179
[62] Tauc J, Grigorovici R and Vancu A 1966 *Phys. Status Solidi (b)* **15** 627
[63] Zhang Y and Pan C 2011 *J. Mat. Sci.* **46** 2622
[64] Lv T, Pan L, Liu X, Lu T, Zhu G, Sun Z *et al* 2012 *Catal. Sci. Technol*. **2** 754
[65] Zeng P, Zhang Q, Peng T and Zhang X 2011 *Phys. Chem. Chem. Phys.***13** 21496
[66] Baeissa E S 2014 *Ceram. Inter.* **40** 12431
[67] Li X, Wen J, Low J, Fang Y and Yu J 2014 *Sci. China Mater.* **57** 70
[68] Yang X, Xiao T and Edwards P P 2011 *Int. J. Hydrogen Energ.* **36** 6546
[69] Nakata K and Fujishima A 2012 *J. Photochem. Photobiol. C: Photochem. Rev.* **13** 169
[70] Linsebigler A L, Lu G and Yates J T 1995 *Chem. Rev.* **95** 735
[71] Wu J C 2009 *Catal. Surv. Asia* **13** 30
[72] Tseng I-H and Wu J C-S 2004 *Catal. Today* **97** 113
[73] Hsu H C, Shown I, Wei H-Y, Chang Y C, Du H Y, Lin Y G *et al* 2013 *Nanoscale* **5** 262
[74] Sun M, Liu H, Liu Y, Qu J and Li J 2015 *Nanoscale* **7** 1250
[75] Schneider J, Jia H, Muckerman J T and Fujita E 2012 *Chem. Soc. Rev.* **41** 2036